NATIONAL ENERGY TECHNOLOGY LABORATORY

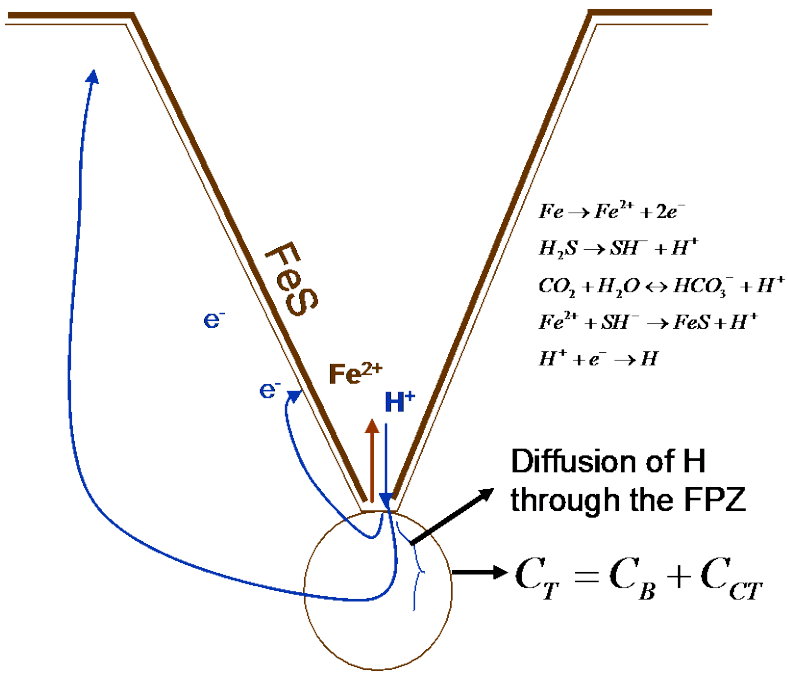

Fatigue Crack Growth Rate of UD-165 in Sour Environments

3 December 2013

U.S. DEPARTMENT OF ENERGY

Office of Fossil Energy

NETL-TRS-3-2013

Disclaimer

This report was prepared as an account of work sponsored by an agency of the United States Government. Neither the United States Government nor any agency thereof, nor any of their employees, makes any warranty, express or implied, or assumes any legal liability or responsibility for the accuracy, completeness, or usefulness of any information, apparatus, product, or process disclosed, or represents that its use would not infringe privately owned rights. Reference therein to any specific commercial product, process, or service by trade name, trademark, manufacturer, or otherwise does not necessarily constitute or imply its endorsement, recommendation, or favoring by the United States Government or any agency thereof. The views and opinions of authors expressed therein do not necessarily state or reflect those of the United States Government or any agency thereof.

Cover Illustration: Schematic depiction of the crack tip system.

Suggested Citation: Thodla, R.; Gui, F.; Hawk, J. A. *Fatigue Crack Growth Rate of UD-165 in Sour Environments*; NETL-TRS-3-2013; EPAct Technical Report Series; U.S. Department of Energy, National Energy Technology Laboratory: Morgantown, WV, 2013; p 32.

An electronic version of this report can be found at: http://netl.doe.gov/onsite_research

Fatigue Crack Growth Rate of UD-165 in Sour Environments

Ramgopal Thodla[1], Feng Gui[1], Jeffrey A. Hawk[2]

[1]DNV USA, 5777 Frantz Road, Dublin, OH 43017

[2]U.S. Department of Energy, National Energy Technology Laboratory, 1450 Queen Avenue SW, Albany, OR 97321

NETL-TRS-3-2013

3 December 2013

NETL Contacts:

Jeffrey Hawk, Principal Investigator

Kelly Rose, Technical Coordinator

George Guthrie, Focus Area Lead

This page intentionally left blank

Table of Contents

EXECUTIVE SUMMARY **1**
1. BACKGROUND **3**
2. LITERATURE REVIEW **5**
3. EXPERIMENTAL **8**
3.1 FGCR TEST METHOD AND MEASUREMENT 8
4. RESULTS AND DISCUSSION **11**
4.1 MATERIALS CHARACTERIZATION 11
4.2 FCGR TESTS AT 20°C 11
4.3 FCGR TESTS AT 85°C 14
4.4 FCGR TEST AT 200°C 15
4.5 ANALYTICAL MODELS FOR ENVIRONMENTALLY ASSISTED FCGR 16
5. CONCLUSION **21**
6. REFERENCES **23**

List of Figures

Figure 1: Schematic depiction of the crack tip system. C_T is the total hydrogen in the crack tip, C_B is the hydrogen concentration from bulk charging, C_{CT} is the hydrogen charged into the fracture process zone from the crack tip. 6
Figure 2: Schematic representation of crack growth measurements in environment. 9
Figure 3: Microstructure of a) S-135 and b) UD-165 etched with Nital (2 wt.% nitric acid in ethanol). 11
Figure 4: FCGR as a function of frequency for UD-165 at pH = 7 and 20°C under various conditions. 12
Figure 5: FCGR as a function of frequency for UD-165 at pH = 9 and 20ºC under various partial pressure H_2S conditions. 13
Figure 6: FCGR as a function of frequency for UD-165 at pH = 12 and 20ºC under various conditions. 13
Figure 7: FCGR as a function of frequency for UD-165 at 85ºC under various conditions..... 14
Figure 8: Comparison of FCGR at pH = 7 as a function p_{H2S} and temperature..... 15
Figure 9: Fatigue crack growth of UD-165 at 200ºC; pH = 7; p_{H2S} = 0.12 psia; and ΔK = 10 ksi√in..... 16
Figure 10: Effect of hydrogen diffusion co-efficient on the ratio C_{crit}/C_s from the results of the various tests performed. 20

List of Tables

Table 1: Typical mechanical properties for S-135 and UD-165 drill pipe 8
Table 2: Alloying elements for S-135 and UD-165 drill pipe (in wt.%) 8
Table 3: Matrix for FCGR testing. All tests performed were frequency scan tests with frequencies ranging from 3 Hz to 1 mHz..... 10
Table 4: Results of the fit of Af^n with n = -½ to the FCGR vs. frequency data..... 19

Acronyms and Abbreviations

Term	Description
API	American Petroleum Institute
ASTM	American Society for Testing and Materials
BHA	Bottom hole assembly
CT	Compact tension
DCPD	Direct current potential drop
DOE	Department of Energy
DMM	Digital multimeter
DNV	Det Norske Veritas
EDM	Electro discharge machining
EDS	Energy dispersive spectroscopy
ERD	Extended reach drilling
FCGR	Fatigue crack growth rate
FPZ	Fracture process zone
HTHP	High temperature, high pressure
NETL	National Energy Technology Laboratory
pH	Decimal *logarithm* of the reciprocal of the H ion activity, $a_{H}+$, in a solution
psia	Pounds per square inch absolute
PTFE	Polytetrafluoroethylene
SCC	Stress corrosion cracking
SCE	Saturated calomel electrode
SSC	Sulfide stress cracking
TiDP	Titanium drill pipe
WDS	Wavelength dispersive spectroscopy

Symbols

Symbol	Definition and Unit
Δa	Critical embrittlement distance of a growing crack
a	Crack length
(a/W)	Ratio of actual crack length to total possible crack length
A	Constant in frequency response $A f^n$ used to describe FCGR
C_B	Hydrogen concentration from bulk charging
C_{crit}	Critical hydrogen concentration required for crack growth
C_{CT}	Hydrogen charged into the fracture process zone from the crack tip
C_s	Concentration of hydrogen in the lattice in equilibrium with crack tip
C_T	Total hydrogen in the crack tip
C_x	Concentration of hydrogen at distance *x* from fracture process zone
D_{eff}	Effective diffusion coefficient
D_H	Diffusion co-efficient of hydrogen
erf	Error function
f	Frequency (Hz)
i	Current density associated with hydrogen generation
i_o	Exchange current density of the reaction
k	Constant (Equation 3)
K	Stress intensity factor
K_{ISCC}	Critical value to produce crack growth by stress corrosion cracking
K_{max}	Maximum stress intensity factor
K_{min}	Minimum stress intensity factor
n	Variable in frequency response Af^n related to FCGR mechanism
p_{H2S}	Partial pressure H_2S
pH	Decimal logarithm of the reciprocal of hydrogen ion activity
q	Charge passed in one half of the frequency cycle
q_s	Saturation charge for the reaction
R	Ratio of K_{min} / K_{max}
t	Time
τ	Characteristic frequency (Hz)

Acknowledgments

This work was completed as part of National Energy Technology Laboratory (NETL) research for the Department of Energy's (DOE) Complementary Research Program under Section 999 of the Energy Policy Act (EPAct) of 2005. The authors wish to acknowledge Roy Long (NETL Strategic Center for Natural Gas and Oil) and Elena Melchert (DOE Office of Fossil Energy) for programmatic guidance, direction, and support.

The authors also wish to acknowledge the contribution of Scott Harrold in performing the laboratory tests.

This page intentionally left blank

EXECUTIVE SUMMARY

Materials failures are a concern associated with the high temperature, high pressure (HTHP) sour environments encountered in deep well drilling, completion, and production operations. The pressure (> 30 ksi), temperature (> 500°F), and corrosive constituents (> 5 ppm H_2S) in the well environment can result in general corrosion, stress corrosion cracking (SCC), sulfide stress cracking (SSC), pitting corrosion, fatigue failures, and significant wear on components. Consequently, alloys utilized in these applications must have high yield strength, excellent fatigue capability, and excellent toughness with good to excellent corrosion resistance, and in drilling operation, very good wear resistance. It is critical to understand the relationships between metallurgical factors and microstructure which affect mechanical behavior in order to evaluate alloys for use in these extreme environments and thus, ameliorate the incidents of catastrophic failure, especially in the presence of corrosive species that act to degrade material integrity. Ultra-deep (>20,000 ft) environments uniquely pose significant challenges for materials used in drilling, completion, and production where service life can be compromised by the aforementioned factors.

Data at these depths is sparse but where available on materials in wells <25,000 ft indicate that H_2S and CO_2 corrosion, as well as abrasive wear, are problems for tubular products, including drill pipe, casing and tool joints, and drilling risers. A very critical corrosion component in H_2S containing sour gas environment is sulfide stress cracking, which may cause sudden brittle fracture. Also, catastrophic failure can be caused by fatigue. Since failure mechanisms are different for sulfide stress cracking and/or hydrogen embrittlement (tensile stress) and corrosion assisted fatigue (cyclic stress), it is of utmost importance to understand the susceptibility of the different materials used in deep sour environments and to evaluate the potential failure modes.

A program was conducted to understand the performance of UD-165, an ultra-high strength, low-alloy steel, for drill pipe application in sour environments where temperature, environment pH, and H_2S partial pressure as well as selected mechanical testing factors were varied (such as frequency of cyclic stress, which was used to simulate a range of operational conditions). The results of the program are summarized below and provide guidance as to important factors that influence fatigue performance in terms of crack growth rate in ultra-deep well sour environments:

- Fatigue crack growth rate (FCGR) of UD-165 in sour environments increased with decreasing frequency of cyclic stress in a range of environmental conditions at pH = 7, over a frequency range of $1x10^{-3}$ Hz to $3x10^{0}$ Hz. The FCGR vs. frequency plot exhibited a slope of -0.5.
- In higher pH environments, pH = 9 and pH = 12, the FCGR did not exhibit a strong frequency dependence either due to the mild environmental conditions or due to crack closure phenomenon
- At an elevated temperature of 200°C, the FCGR vs. frequency at pH = 7 had a slope of -1, suggesting a change in mechanism from hydrogen diffusion to that of stress corrosion cracking
- The data from the experimental program were fit to an analytical model which suggests that the rate limiting step in fatigue crack propagation under the test conditions used in this study is hydrogen diffusion through the fracture process zone

The information from this test program and resulting analysis of environmental effects on crack growth will provide guidance in selecting materials for these applications and be useful in determining the bounds for their use in ultra-deep environments.

1. BACKGROUND

As drilling conditions become harsher, there is a greater demand for high-strength materials to increase the strength to weight ratio of the pipe. There have been developments in the area of low alloy steels with strengths as high as 135 ksi. High-strength steels represent a near-, mid-, and long-term technology for extended reach drilling (ERD). Current high-strength grades available on the market today are Z-140 and V-150. These grades provide 4% and 11% improvement in strength-to-weight ratio, respectively, compared to S-135 drill pipe, and carry only a relatively small cost premium over S-135 drill pipe. There are, in general, concerns associated with adopting high-strength grades primarily due to issues regarding reduced ductility and toughness of the steel. However, manufacturers have significantly improved the pipe manufacturing technology and can now offer these grades with toughness levels better than S-135 drill pipe processed to standard American Petroleum Institute (API) specifications. The substantial improvement in obtaining high toughness in high-strength steels has led drill pipe manufacturers to develop ultra-high strength steels, such as UD-165. UD-165 is an ultra-high strength, low-alloy steel for drill pipe application in sour environments where temperature, environment pH, and H_2S partial pressure as well as selected mechanical testing factors were varied. The development of a UD-165 grade with 165 ksi yield strength tubes would provide a 22% improvement in strength-to-weight ratio compared to S-135 drill pipe. This would be second only to titanium drill pipe (TiDP) by 15% in strength-to-weight ratio. It is likely that the cost of UD-165 would be substantially less than TiDP.

Offshore drilling operations are very costly (Macdonald and Bjune, 2007). A drillstring failure, for example, will have severe economic consequences with typical day-rate for drilling operations (until recently) at a fixed production installation averaging about $100,000. If on the other hand the drillstring failure occurs on a floating deep-water exploration platform, these per day costs could easily be twice as much. However, the present high oil prices and associated increased costs in exploration and production activity can push these costs ever higher, for example, they can exceed $400,000 per day (mid-2006) for deep-water drilling operations (i.e., rigs drilling at depths > 5,000 ft).

As far back as 1985, it was reported that 45% of deep well drilling problems were related to drillstring failures with another report concluding that drillstring separations occurred in one in seven wells (Vaisberg et al., 2002). Of the drillstring separations, 36% were due to stuck pipe. For example, from 2001 to 2002 total costs due to stuck pipe for the worldwide drilling industry ranged as high as $250 million (calculated over a 15-month period, although the exact dates were not stated; Vaisberg et al., 2002).

Another survey of drilling problems reported worldwide from 1987 through 1990, focused on 76 individual drillstring failures. The results of the survey showed that torsion and tension failures accounted for 13%, while fatigue was specifically cited in 50 of the 76 failures (65%). Fatigue as a mechanism also contributed significantly in 10 other failures within this group (Vaisberg et al., 2002). Fatigue damage is usually due to reversal in the stress state of an object; for example, when a tensile type specimen is first loaded in tension and then loaded in compression. In the drilling environment this is analogous to when the drill pipe rotates in a curved section of a wellbore going from tension to compression as the pipe rotates. However, more catastrophic failures can occur, for example, when rotating a buckled pipe. This may quickly lead to rapid fatigue failure. While fatigue is clearly an important issue, the combination of fatigue stresses in

the presence of sour conditions clearly has an important effect on the design and operating regimes of drill pipes.

The reason a drillstring failure, defined as the complete separation of the drillstring or the bottom hole assembly (BHA), is so costly is that in extreme cases it may be necessary to drill a new hole parallel to the section occupied by the abandoned drillstring, where it is not possible to recover the remaining equipment (termed “fishing”). Depending on the depth where drillstring failure occurred, a sidetrack operation of this nature could take from a few days to more than a dozen to complete. The cost alone of replacing lost equipment can easily exceed $1 million. The cost ratio for detecting the impending failure before final separation, the so called leak-before-break state, is dramatic at 10:1 (Macdonald and Bjune, 2007). By detecting a wash-out prior to twist-off, immense cost savings can be realized. Alternatively, if better understanding of corrosion-fatigue and the rate of crack growth in the drillstring can be realized for the various deep-water environments, then more frequent and comprehensive inspection protocols can be engaged to search for changes related to leakage in the drillstring before complete separation occurs.

2. LITERATURE REVIEW

In certain situations corrosion fatigue may occur. As an example consider C-Mn steels in sour environments where concern arises in various offshore applications because periodic forces come into play, such as for wave motion and subsurface current flow that affect flowlines and risers. The commonly accepted mechanism of fatigue crack growth rate (FCGR) behavior in these environments is believed to be hydrogen-enhanced FCGR. The effect of H_2S on steels is typically observed as an increase in the FCGR, with typical FCGR at high ΔK values being as high as 50 times their equivalent values in air (e.g., Vaisberg et al., 2002; Webster et al., 1985; Bristoll and Roeleveld, 1978; Eadie and Szklarz, 1999a; Eadie and Szklarz, 1999b; Maddox et al., 2005; Eadie et al., 2003; Buitrago et al., 2004).

Fatigue crack growth rate studies in a range of environments indicate that FCGR increases with increasing H_2S concentration (Vaisberg et al., 2002; Bristoll and Roeleveld, 1978; Eadie and Szklarz, 1999a; Eadie and Szklarz, 1999b; Maddox et al., 2005). The effect of low ΔK leads to a slower increase in the FCGR over those determined in air as compared to high ΔK. The threshold limit is not strongly influenced by the specific environment. Another important effect of sour environments on FCGR is the cycle frequency; usually it is found that with decreasing frequency, the FCGR increases and reaches a plateau (Buitrago et al., 2004; Hammond and Baxter, 2008; Thodla et al., 2010). FCGR measurements performed in a range of environments from gaseous hydrogen to distilled water exhibited this behavior (Gangloff, 1990; Wei and Gangloff, 1989; Wei and Shim, 1983).

Wei and Gangloff developed a significant understanding of the corrosion-fatigue process by trying to understand what was occurring at the crack tip (Gangloff, 1990; Wei and Gangloff, 1989; Wei and Shim, 1983). The crack tip region can be modeled schematically as shown in Figure 1. The hydrogen generation reaction leads to adsorption, followed by absorption of hydrogen atoms in the metal. H_2S strongly enhances the absorption of hydrogen atoms by preventing their recombination as H_2. The absorbed hydrogen typically diffuses to the fracture zone and causes embrittlement. The possible rate controlling steps in the hydrogen-related fatigue process are:

- Surface reactions generating hydrogen
- Diffusion of hydrogen through the fracture zone
- Stress corrosion cracking controlled growth

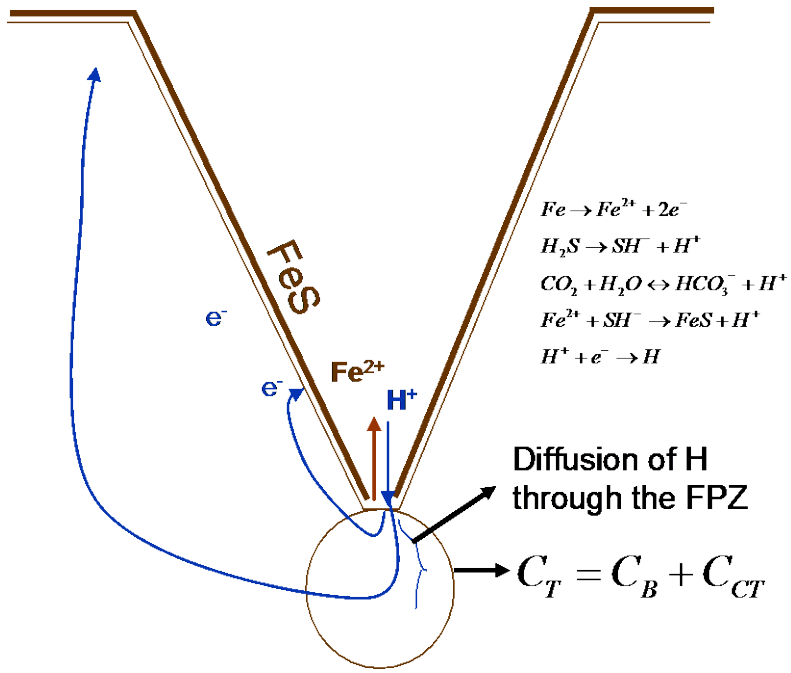

Figure 1: Schematic depiction of the crack tip system. C_T is the total hydrogen in the crack tip, C_B is the hydrogen concentration from bulk charging, C_{CT} is the hydrogen charged into the fracture process zone from the crack tip.

Corrosion fatigue of steels has been studied in gaseous H_2S environments and under cathodic polarization in sea water environments. A significant amount of work in gaseous environments performed by Wei and co-workers has lead to the development of the surface reaction based model for FCGR (Gangloff, 1990; Wei and Gangloff, 1989; Wei and Shim, 1983). The surface reaction model essentially assumes that the rate of mass transport, surface mobility, and diffusion of hydrogen through the fracture process zone (FPZ) to be rapid. It considers the rate of reactions at the crack tip to be the rate limiting step.

In order to account for various possible mechanisms, as well as to test the applicability of these mechanisms, it is instructive to look at the corrosion fatigue process via the superposition principle proposed by Wei and Gangloff (Gangloff, 1990; Wei and Gangloff, 1989; Wei and Shim, 1983). Under this principle, corrosion fatigue process can be completely represented by sum of FCGR in air, corrosion fatigue, and stress corrosion cracking (SCC).

The surface reaction model assumes that the rate limiting step in the FCGR is the reaction rate of the bare metal exposed at the crack tip during the fatigue process. In this model, it is proposed that the FCGR is related to the volume of hydrogen generated during the surface reaction. The volume of hydrogen was estimated based on the cumulative charge passed when fresh metal was exposed. This hypothesis was tested by measuring the charge passed during repassivation measurements performed on a freshly exposed surface obtained by rapid straining tensile specimens in environments. The charge density associated with the repassivation transient of the freshly exposed metal increased with time before plateauing. The increase in charge density with time was consistent with increasing FCGR with decreasing frequency. However, it is important to point out that the repassivation experiments were performed in bulk environments, as opposed to crack tip chemistry conditions, where the fresh metal would be exposed during the loading cycle. This model does not account for the micromechanics of fatigue crack propagation through

the fracture process zone. The model also does not account for the role of bulk charging vs. local crack tip charging.

The role of hydrogen diffusion through the fracture process zone as the rate limiting step in FCGR of steels under various conditions has been developed to account for the observations of FCGR. The increase in FCGR with decreasing frequency has been attributed to insufficient time for hydrogen diffusion through the fracture process zone at higher frequencies. At sufficiently low frequencies there is sufficient time for the hydrogen to diffuse through the fracture process zone leading to a plateau in the FCGR. The FCGR plateau at different values of ΔK was related to $1/\sqrt{f_{plateau}}$, which was further evidence of FCGR being driven by the diffusion of hydrogen through the fracture process zone (Gangloff, 1990). The role of hydrogen diffusion as the rate controlling step has been proposed for aluminum alloys in chloride-containing environments, where the FCGR was proportional to $1/\sqrt{f_{plateau}}$ (Krishnamurthy, 1991).

A significant amount of work has been performed in steels under cathodic polarization in seawater (Turnbull and Saenz de Sanata Maria, 1988; Turnbull et al., 1988; Turnbull, 1986). Turnbull investigated the crack tip chemistry of BS7410 under various loading conditions as well as potentials ranging from corrosion potential to -1200 mV vs. a saturated calomel electrode (SCE) (Turnbull, 1986). The primary finding of this work indicated the crack tip chemistry in steels was slightly alkaline. This was rationalized on the basis that metal dissolution at the crack tip was supported largely by cathodic reactions on adjacent crack walls. It was also found that the dominant source of hydrogen was from bulk charging at -900 mV (vs. SCE) and 0.1 Hz. Thus, the role of crack tip charging was insignificant.

In H_2S environments, the formation of FeS leads to the decay of the hydrogen concentration on the entry surface, and thus, leads to non-uniform hydrogen concentration through the thickness of the specimen. In this case, shallow cracks close to the surface will likely have a higher concentration of hydrogen than will deeper cracks (Holtam, 2009). The results obtained at constant ΔK and at 0.1 Hz in sour environments indicated a decreasing FCGR with increasing depth, again suggesting that bulk hydrogen plays an important role as opposed to hydrogen charging from the crack tip. Fatigue crack growth rate in sour environments (e.g., pH = 3.5; 7 wt% H_2S) performed under increasing ΔK showed higher FCGR than under decreasing ΔK (Holtam et al., 2009). The difference in behavior was attributed to very shallow cracks that formed during the increasing ΔK portion of the test. Under these conditions, it was proposed that a greater concentration of diffusible hydrogen existed in the crack tip region compared to what was available to deeper cracks during the decreasing ΔK portion of the curve (Holtam et al., 2009).

Until this study only limited work has been performed on the effect of sour environments on high-strength steels used for drilling applications. Research contained herein is aimed at understanding the FCGR behavior of UD-165 in drilling environments over a range of environmental conditions (pH and H_2S partial pressure) and temperatures.

3. EXPERIMENTAL

Roughly 3-m length of UD-165 drill pipe (NOV Grant Prideco, Navasota, TX) was obtained for this study. Tensile testing results were provided by the manufacturer for the heat of UD-165 examined in this study. Those results are given in Table 1. For comparison purposes test data for S-135 (standard drill pipe) are also included. Rockwell C hardness testing was done according to ASTM standard E-18 (ASTM Standard E18, 2008), and is compared to S-135. The chemical composition for UD-165 was determined using combustion-infrared absorbance (S and C), inert gas fusion-thermal conductivity (N), and inductively coupled plasma atomic emission spectroscopy for all other elements (ASTM Standard E1019, 2008). The nominal chemistry for a representative sample of S-135 has also been provided. The results of the chemistry determinations for S-135 and UD-165 are found in Table 2. Additionally, samples of both S-135 and UD-165 were machined and polished to a 0.05 μm finish before being etched with Nital (2wt.% nitric acid in ethanol) to observe the microstructures.

Table 1: Typical mechanical properties for S-135 and UD-165 drill pipe

Property	Yield Strength (ksi)	Ultimate Tensile Strength (ksi)	Elongation (%)	Hardness (HRC)
S-135	155.5	168.7	19.2	35.1 ± 0.13
UD-165	175.6	182.5	58.5	40.1 ± 0.16

Table 2: Alloying elements for S-135 and UD-165 drill pipe (in wt.%)

Element	Al	B	C	Cr	Cu	Mn	Mo	N
S-135	0.03	<0.005	0.26	1.39	0.02	0.78	0.68	0.005
UD-165	0.03	<0.005	0.27	0.79	0.19	0.88	0.67	0.007
Element	**Nb**	**Ni**	**P**	**S**	**Si**	**Sn**	**Ti**	**V**
S-135	<0.01	0.02	0.006	0.002	0.3	<0.01	<0.01	<0.01
UD-165	0.02	0.81	<.005	0.007	0.26	<0.01	<0.01	0.07

Fatigue crack growth rate experiments were performed on compact tension (CT) specimens extracted from UD-165 pipe. The research contained herein utilized the following size of CT specimens: ½T-CT specimens with B = 0.1875″.

3.1 FGCR TEST METHOD AND MEASUREMENT

The pipe sections of UD-165 were supplied to Det Norske Veritas (DNV) by National Energy Technology Laboratory (NETL). This study used ½T-CT specimens, which were extracted with the crack oriented through the thickness of the pipe. The specimens were machined with an Electro

Discharge Machining (EDM) notch of 0.25″ and pre-cracked to an a/W ratio of 0.35 at a ΔK of 15 ksi√in. All experiments were performed on servo electric load frames, with the crack growth distance measured using direct current potential drop (DCPD) technique. In this technique, a constant current of 4 A was applied cross the crack opening with the voltage drop across the crack opening measured using a high resolution digital multimeter (DMM). The current source used was an Agilent 6611C with voltage measurements performed using a NI-PXI1033 chassis equipped with NI-PXI4071 DMM and NI-PXI2527 Switch. Platinum wires of 0.020″ and 0.040″ were used for voltage and current probes, respectively. The Pt wires were heat shrunk in polytetrafluoroethylene (PTFE) to prevent contact with the cell and the solution. The spot weld locations of the probes on the samples were also coated with Epoxy Systems™ Product 641 to prevent corrosion around the probes. The voltage drop measured during testing was converted into crack length using the Johnson equation (ASTM E399, 2009). Crack growth conversion was programmed in LabView® and was used to calculate the crack length, which was then used during the FCGR test to adjust the load to either maintain a constant K or to impose a variable K. Changes in the load were made only when the crack length increased.

The electrochemical test cell and the test solution were both deaerated with high purity nitrogen. The oxygen level in the test solution was confirmed to be below 10 ppb using an oxygen probe (Hamilton Visiferm 120) before switching to the test gas. The solution was saturated with the test gas and then re-circulated through the test cell. All samples were then soaked in the test cell for three days prior to performing the corrosion fatigue crack growth measurements, according to the conditions in Table 3. The pH was maintained at a value of 7 by using $CO_2/NaHCO_3$ equilibrium, whereas the higher values of pH, i.e., 9 and 12, were maintained using $NaHCO_3/Na_2CO_3$ equilibrium. The test program was designed to explore the effects of pH, partial pressure of H_2S (p_{H2S}) and temperature. A series of tests were also performed at room temperature to explore the effect of ΔK. All samples except one were tested without coating to maximize the amount of hydrogen in the sample for a given environment. Figure 2 shows a schematic diagram of the representative electrochemical test system.

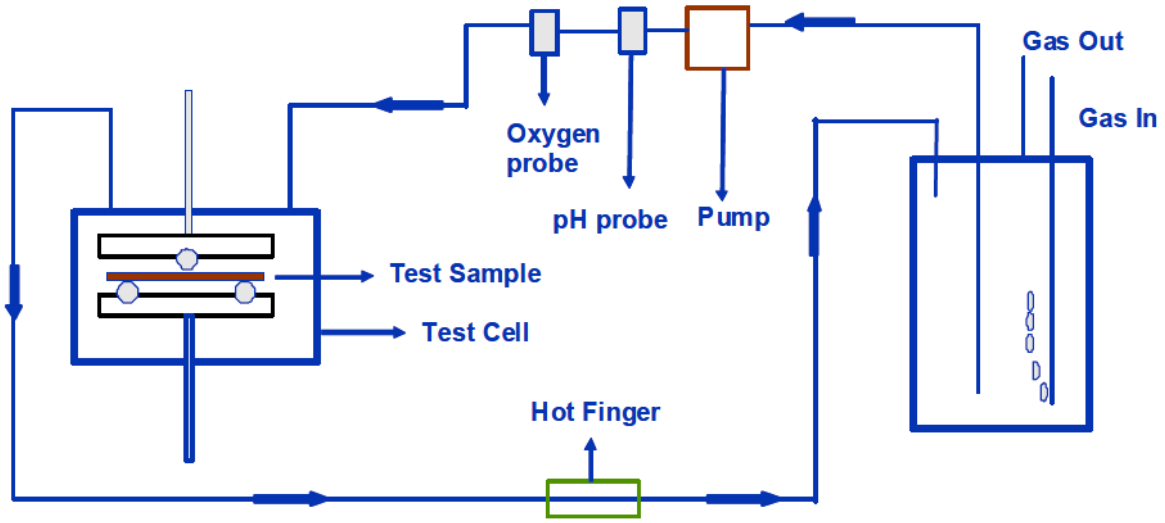

Figure 2: Schematic representation of crack growth measurements in environment.

Table 3: Matrix for FCGR testing. All tests performed were frequency scan tests with frequencies ranging from 3 Hz to 1 mHz

Environment			Mechanical Variables		Coating
pH	p_{H2S} (psia)	Temperature (C)	ΔK (ksi√in)	R-ratio (K_{max}/K_{min})	Y/N
7	0.12	20	28	0.13	N
7	1.2	20	28	0.13	N
7	10	20	28	0.13	N
9	0.12	20	28	0.13	N
9	1.2	20	28	0.13	N
9	10	20	28	0.13	N
12	0.12	20	28	0.13	N
12	1.2	20	28	0.13	N
12	10	20	28	0.13	N
7	0.12	85	28	0.13	N
7	1.2	85	28	0.13	N
7	10	85	28	0.13	N
9	0.12	85	28	0.13	N
9	1.2	85	28	0.13	N
9	10	85	28	0.13	N
12	0.12	85	28	0.13	N
7	0.12	200	10	0.5	N
7	0.12	20	10	0.5	N
7	0.12	20	20	0.13	N
7	0.12	20	13.97	0.13	N
7	0.12	20	28	0.13	Y

4. RESULTS AND DISCUSSION

4.1 MATERIALS CHARACTERIZATION

The mean values of ten Rockwell C hardness tests are shown in Table 1 for each alloy. Table 2 shows the chemical analysis results while Figure 3 shows the microstructures of the two alloys. Both alloys have martensitic microstructures, while the UD-165 suggests a finer prior austenite grain size relative to S-135. Sulfur levels were low (Table 1) and while manganese containing sulfide inclusions were identified in both alloys by energy dispersive spectroscopy (EDS) and wavelength dispersive spectroscopy (WDS), they were not common. The most commonly observed inclusions were oxides containing Si sometimes with Mg and/or Ca. Sulfur was commonly also observed at the oxide inclusions.

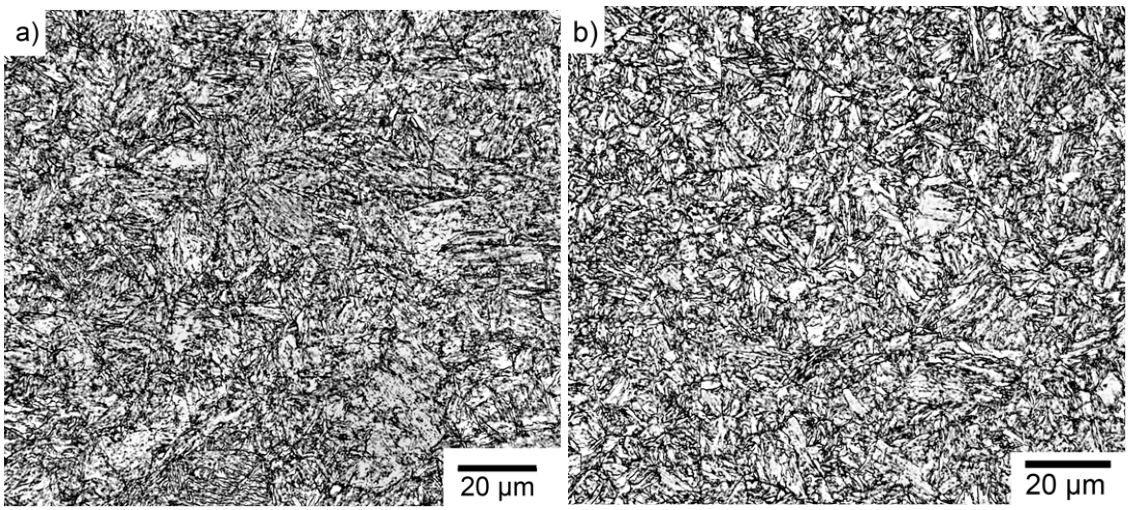

Figure 3: Microstructure of a) S-135 and b) UD-165 etched with Nital (2 wt.% nitric acid in ethanol).

4.2 FCGR TESTS AT 20°C

The results of the FCGR vs. frequency at pH = 7 and 20°C are shown in Figure 4. While a fatigue crack growth frequency scan test was attempted at pH = 7 and partial pressure of H_2S of 10 psia, the test resulted in brittle fracture when loading to K_{max} = 33 ksi√in, suggesting that under these conditions the K_{1SCC} was lower than 33 ksi√in. In all experiments FCGR increased with decreasing frequency, indicating a strong environmental effect.

The FCGR at p_{H2S} of 0.12 psia and 1.2 psia at 28.7 ksi√in are very similar. No evidence of a plateau in these sets of data was observed. For the case of the coated sample tested at a starting stress intensity of 28.7 ksi√in, there was evidence of a plateau region at a frequency of about 3 mHz. It is interesting to note that the FCGR for the coated sample is lower than that of the uncoated sample under identical test conditions. The only difference amongst the experiments is that the coated sample had a smaller exposed region to the solution environment. This led to enhanced cathodic activity, and hence, there was a lower concentration of diffusible hydrogen available to the growing crack. This lower concentration of diffusible hydrogen may be responsible for the lowered FCGR on the coated sample. At a ΔK level of 20 ksi√in a plateau

was observed at about 30 mHz. At ΔK levels of 13.97 ksi√in and 10ksi√in plateaus at higher frequencies were seen in the range of about 300 mHz.

An important aspect of the data is that the FCGR has a $f^{-0.5}$ dependence on the frequency. The lines on the graph represent the fit to the data using an equation of the form Af^{n}. The equation utilized a value for n = -0.5 to fit the data. The values of the A are shown on the graph. It is evident from the data that with decreasing ΔK, FCGR also decreases.

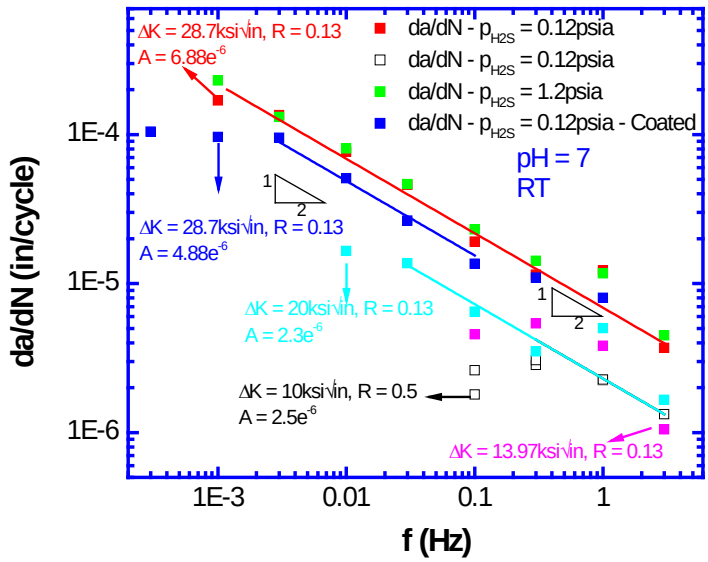

Figure 4: FCGR as a function of frequency for UD-165 at pH = 7 and 20°C under various conditions.

The results of the FCGR vs. frequency at pH =9 and 20°C are shown in Figure 5. For these tests, FCGR increases as function of frequency for the lowest concentration of H_2S (i.e., p_{H2S} = 0.12 psia). The FCGR at pH = 9 are similar to the results at pH = 7, i.e., they too have a $f^{-0.5}$ dependence on the frequency. The line on the graph represents the fit to the data using an equation of the form Af^{n}, where n was equal to -0.5. The value of the A for this curve is again indicated on the graph.

However, with increasing concentrations of H_2S the FCGR does not show the usual dependence on frequency, suggesting that corrosion products or corrosion film may have formed at the higher pH levels due to the insolubility of the iron sulfide and/or iron carbonate species, resulting in crack closure effects that thereby lowers the effective ΔK. This has been observed in sulfide environments at low pH values where voluminous corrosion products/films composed of FeS had formed (Hudak, 2010). The crack closure phenomenon under these conditions masks the usual environmental effect that would normally be expected with increasing H_2S concentration. In the mildest H_2S containing environments, it is likely that the corrosion products/films are not as voluminous, and hence, they are less likely to cause significant crack closure effects. It is anticipated that with increasing H_2S concentration, the atomic hydrogen generated on the surface of the specimen would likely increase if not remain the same; hence, it is unlikely that the frequency independent behavior is due to a decrease in hydrogen concentration in the steel.

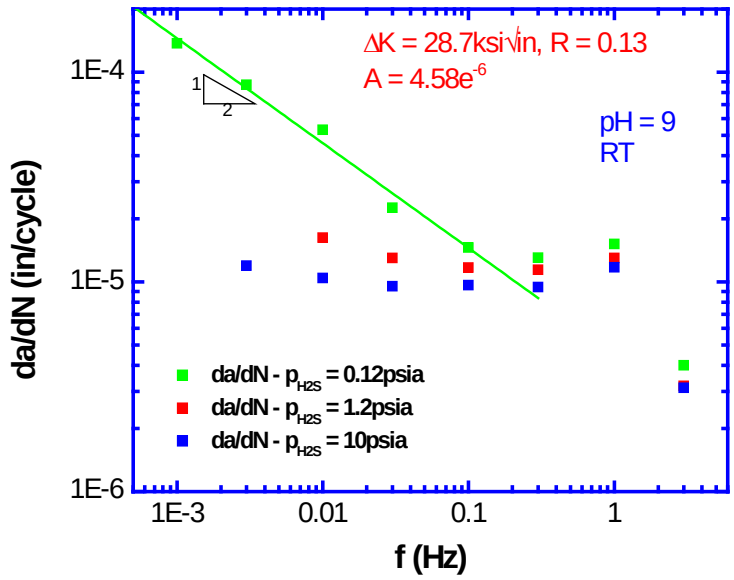

Figure 5: FCGR as a function of frequency for UD-165 at pH = 9 and 20ºC under various partial pressure H_2S conditions.

The results of the FCGR frequency scan tests at pH = 12 and 20°C are shown in Figure 6. In contrast to the results at pH = 7 where FCGR increased with decreasing frequency, FCGR at this pH level was independent of the frequency for all test conditions. This could be due to the more basic pH environment resulting in very low corrosion rates, resulting in a small amount of hydrogen entering the metal. Further, carbonate/sulfide films could form at the crack tip and be responsible for crack closure phenomenon as observed at higher p_{H2S} in pH = 9 environments.

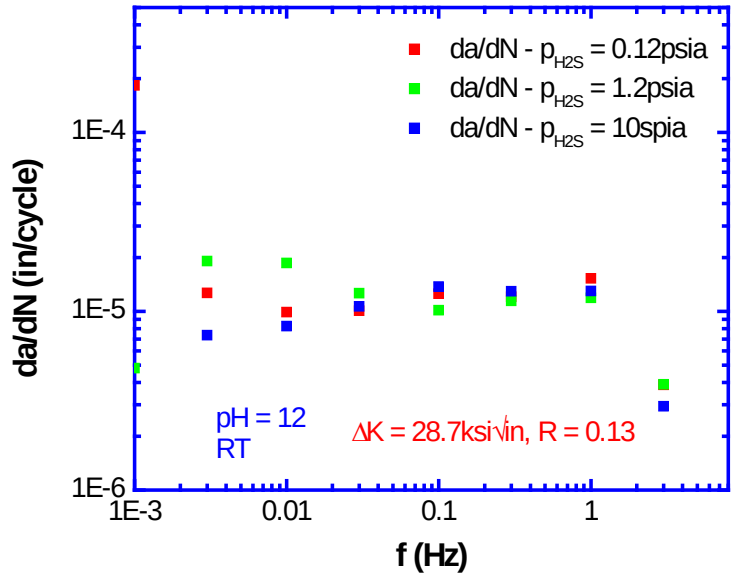

Figure 6: FCGR as a function of frequency for UD-165 at pH = 12 and 20ºC under various conditions.

The results of the FCGR frequency scan tests at room temperature indicate that the environmental effect is strongest at pH = 7. The environmental effect decreases with increasing pH due to the decreased cathodic reaction activity associated with hydrogen generation as well as crack closure effects caused by the formation of corrosion products and/or films that shield the growing crack from the environment.

4.3 FCGR TESTS AT 85°C

The results of the FCGR tests at 85°C are shown in Figure 7. Similar to the tests at 20°C, the FCGR increases with decreasing frequency at pH = 7 over a range of p_{H2S}. At a pH level of 9, the FCGR increases with decreasing frequency only at p_{H2S} of 0.12 psia. At higher levels of p_{H2S}, the FGCR does not show the typical frequency dependence, suggesting that the crack closure phenomenon due to corrosion product/film formation has once again played a significant role in defining the plateau associated with FCGR for these conditions.

A similar set of results was observed at pH of 12. In this series of tests, the FCGR has $f^{-0.5}$ dependence on the frequency, which suggests that hydrogen diffusion may be the rate limiting step. The lines on the graph represent the fit to the data using an equation of the form $A f^{n}$. The equation was fit using n = -0.5. The values of the A are indicated on the graph.

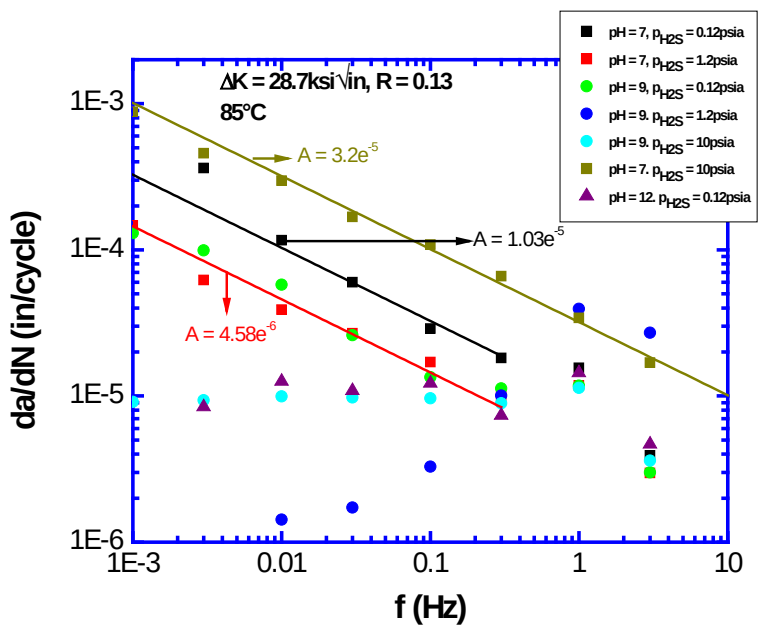

Figure 7: FCGR as a function of frequency for UD-165 at 85ºC under various conditions.

Fatigue crack growth rate frequency scan tests at pH = 7 at the highest p_{H2S} (i.e., 10 psia) show that crack growth rate is significantly higher than at 0.12 psia or 1.2 psia over the entire range of frequencies. This result is consistent with the observation that in increasing concentrations of H_2S, the diffusible hydrogen concentration increases.

Another interesting aspect of the tests was that while the test at 20°C resulted in brittle failure at K_{max} = 33 ksi√in for the test at 10 psi H_2S, no brittle failure was observed at 85°C at the same K value. This result suggests that there is an increase in K_{1SCC} with increasing temperature. This

would also be consistent with the fact that when temperature increases, the diffusion co-efficient also increases, allowing hydrogen to diffuse at a faster rate. This would then account for the increase in K_{1SCC}.

A comparison of the FCGR as a function of frequency at 20°C and 85°C is shown in Figure 8. The magnitude of FCGR over the range of frequencies tested falls within a factor of 2 for those tests performed at p_{H2S} equal to 0.12 psia and 1.2 psia.

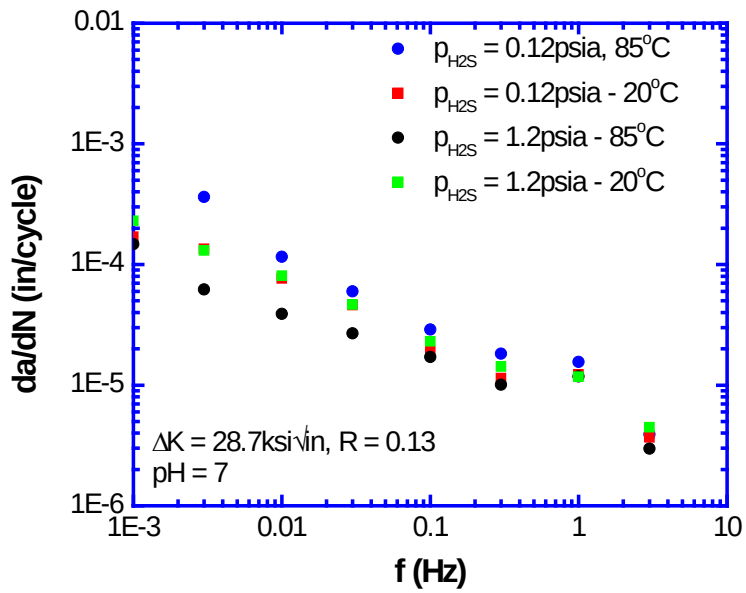

Figure 8: Comparison of FCGR at pH = 7 as a function p_{H2S} and temperature.

4.4 FCGR TEST AT 200°C

A single FCGR frequency scan test was performed at 200°C at a value of ΔK = 10 ksi√in. The results of this test are shown in Figure 9. Crack growth rate increases with decreasing frequency. However, the slope of FCGR vs. frequency curve has a functional dependence different from -½, i.e., the frequency dependence varies as $f^{-0.87}$. This result suggests that the FCGR is likely controlled by a stress corrosion cracking mechanism under these conditions, as opposed to what was discovered at lower temperatures, where FCGR is controlled by hydrogen diffusion.

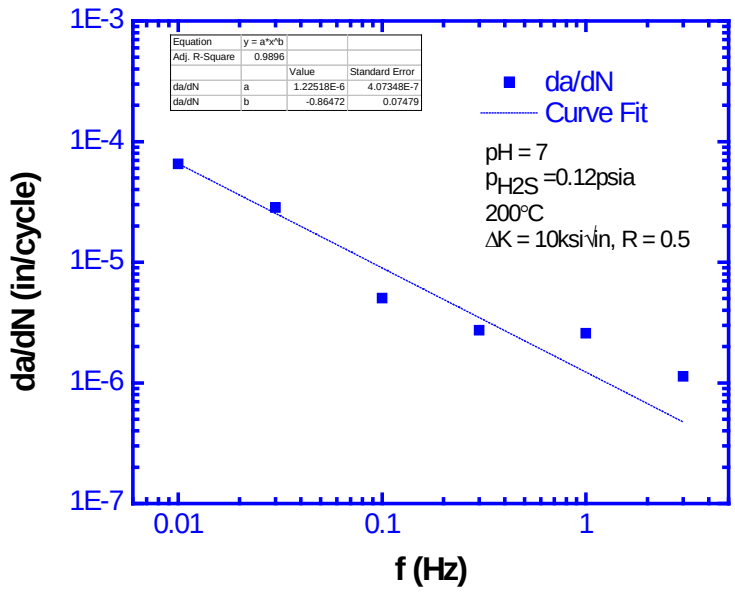

Figure 9: Fatigue crack growth of UD-165 at 200°C; pH = 7; p_{H2S} = 0.12 psia; and ΔK = 10 ksi√in.

4.5 ANALYTICAL MODELS FOR ENVIRONMENTALLY ASSISTED FCGR

Wei and Gangloff developed significant understanding with respect to corrosion fatigue processes by trying to understand processes that occur at the crack tip (Gangloff, 1990; Wei and Gangloff, 1989; Wei and Shim, 1983). Processes that occur at the crack tip can be modeled schematically as shown in Figure 1.

The hydrogen generation reaction leads to adsorption, which is then followed by the absorption of hydrogen atoms into the metal. The absorbed hydrogen typically diffuses to the fracture process zone, and can subsequently result in embrittlement of the alloy. Possible rate controlling steps in the hydrogen-related fatigue process are:

- Surface reactions that generate hydrogen
- Diffusion of hydrogen into the alloy, which then migrates to the fracture process zone
- Interaction of hydrogen with advancing crack tip, leading to stress corrosion cracking controlled growth

In order to account for various possible microscopic mechanisms, as well as testing the applicability of these mechanisms, it is beneficial to look at the corrosion fatigue process using the superposition principle proposed by Wei and Gangloff (Gangloff, 1990; Wei and Gangloff, 1989; Wei and Shim, 1983). They proposed that the corrosion fatigue process could be completely represented by the sum of crack growth rates due, respectively, to ambient conditions (air), corrosion fatigue conditions, and SCC conditions, as shown in Equation 1.

$$(da/dN)_e = (da/dN)_{air} + (da/dN)_{cf} + (da/dN)_{SCC} \quad (1)$$

Thus, if surface reactions are the rate controlling step in the corrosion fatigue process, then $(da/dN)_{cf}$ can be represented by Equation 2, which was developed under the assumption that the crack growth rate is controlled by the volume of hydrogen generated at the crack tip:

$$(da/dN)_{cf} = (da/dN)_{sat} * q/q_s \tag{2}$$

In Equation 2,

$(da/dN)_{sat}$: Saturation value of FCGR

q: Charge passed in a one half of the frequency cycle

q_s: Saturation charge for the reaction

If the rate of the reaction generating hydrogen is assumed to be of the form

$$i = i_o \exp(-kt) \tag{3}$$

where

i: Current density associated with hydrogen generation

i_o: Exchange current density of the reaction

k: Constant

t: Time

then Equation 2 can be integrated and substituted into Equation 3 to give the following result:

$$(da/dN)_{cf} = (da/dN)_{sat} * (1 - \exp(-\tau / f)) \tag{4}$$

In Equation 4,

τ: Characteristic frequency (Hz)

f: Frequency (Hz)

The application of the surface reaction model (i.e., as the rate controlling step) does not support the observations made in this study. In particular, the coated samples and uncoated samples exhibit significantly different plateau FCGR values even though the rate of hydrogen generation at the crack tip is expected to be similar. A significant amount of work has been performed to relate repassivation transients obtained from straining electrode tests to the FCGR vs. frequency relationship to prove this model (Wei and Shim, 1983). It is of note that most of the repassivation transients have been obtained in the bulk environment as opposed to the crack tip environment, and that the role of bulk charging has not been taken into account in this study.

Another possible explanation for crack propagation during corrosion fatigue in a range of environments where hydrogen plays a significant role is based on hydrogen diffusion being the rate limiting step through the FPZ (Gasem, 1999; Gangloff, 2009). In this model, it is assumed that crack propagation occurs when the hydrogen concentration reaches a critical value over a fatigue cycle ($1/f$), reducing the local strength over a distance of Δa in the FPZ to a level that is lower than the stress in the FPZ (Gasem, 1999; Gangloff, 2009). If the concentration of hydrogen at the crack front is assumed constant and fixed, then using a one dimensional diffusion model allows the concentration at any distance to be expressed as:

$$C_x = C_s[1 - erf(x / 2\sqrt{D_H t})] \tag{5}$$

where

C_s: Concentration of hydrogen in the lattice in equilibrium with the crack tip;

C_x: Concentration of hydrogen a distance x from the fracture process zone;

D_H: Diffusion co-efficient of hydrogen

t: Time

The critical embrittlement distance Δa can be estimated when $C_x = C_{crit}$. In this instance C_{crit} is the critical concentration required for the crack to advance:

$$\Delta a = 2\sqrt{D_H t} \times erf^{-1}(1 - C_{crit} / C_s) \tag{6}$$

For discontinous crack propagation (N = 1 cycle), da/dN corresponds to Δa. Thus, when the concentration of hydrogen exceeds C_{crit} the crack growth rate for a cycle is given by

$$da / dN = 2\sqrt{D_H / f} \times erf^{-1}(1 - C_{crit} / C_s) \tag{7}$$

Rearranging as a logarithmic function

$$\log(da / dN) = 1/2 \log(D_H) - 1/2 \log(f) + \log(erf^{-1}(1 - C_{crit} / C_s)) \tag{8}$$

This equation would predict a slope of -0.5 for FCGR vs. f on a log scale. This is in good agreement with the data obtained on all tests that were conducted in this study. The data of FCGR vs. frequency was fit to Af^{n} with n = -0.5.

$$A = D_H^{0.5} \times (erf^{-1}(1 - C_{crit} / C_s) \tag{9}$$

The values of A for the various test conditions are summarized in Table 4. The diffusion coefficient of UD-165 is not known nor is it readily available in literature. Hence the values C_{crit}/C_s are plotted as a function of D_H in Figure 10.

For a high-strength steel with a quenched and temperared martensitic structure, the diffusion co-efficient is assumed to be in the range of $1x10^{-7}$ to $1x10^{-8}$ cm^2/s. Figure 10 suggests that the ratio of the critical concentration of hydrogen for crack propagation compared to the surface concentration decreases in more aggressive conditions (i.e., either in terms of ΔK or the environmental variables). This is consistent with the higher FCGR observed in the more aggressive conditions based on the results of various programs that have been performed by DNV.

Table 4: Results of the fit of Af^{n} with n = -½ to the FCGR vs. frequency data

Environment			Mechanical Variables		Coating	A
pH	p_{H2S} (psia)	Temperature (°C)	ΔK (ksi√in)	R	Y/N	(10^{-6} in/cycle)
7	0.12	20	28	0.13	N	6.9
7	1.2	20	28	0.13	N	6.9
7	10.0	20	28	0.13	N	
9	0.12	20	28	0.13	N	4.6
9	1.2	20	28	0.13	N	
9	10.0	20	28	0.13	N	
12	0.12	20	28	0.13	N	
12	1.2	20	28	0.13	N	
12	10.0	20	28	0.13	N	
7	0.12	85	28	0.13	N	10.3
7	1.2	85	28	0.13	N	4.6
7	10.0	85	28	0.13	N	32.0
9	0.12	85	28	0.13	N	4.6
9	1.2	85	28	0.13	N	
9	10.0	85	28	0.13	N	
12	0.12	85	28	0.13	N	
7	0.12	200	10	0.5	N	
7	0.12	20	10	0.5	N	2.5
7	0.12	20	20	0.13	N	2.3
7	0.12	20	13.97	0.13	N	
7	0.12	20	28	0.13	Y	4.9

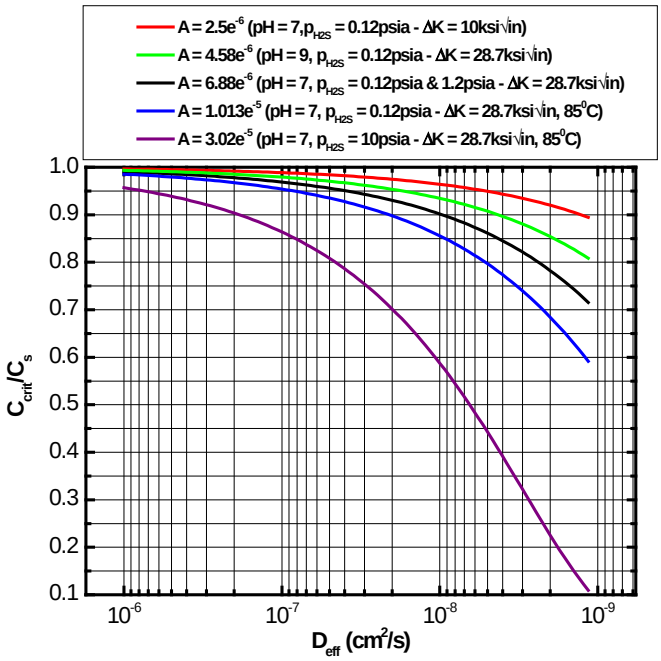

Figure 10: Effect of hydrogen diffusion co-efficient on the ratio C_{crit}/C_s from the results of the various tests performed.

The data on UD-165 in a range of environments indicates that there is no evidence of a plateau at high ΔK, even at frequencies as low as 1 mHz. For example, in environments at pH = 6.5 and a range of p_{H2S} such as 0.12 to 1.2 psia, and identical ΔK, X65 line pipe steel exhibits a plateau in the FCGR at about 10 mHz. It was expected that UD-165 would exhibit similar type of behavior, however, at pH = 7 there is no evidence of plateau at any p_{H2S}.

There are some differences in the nominal chemistry between these two steels but those differences are relatively minor. As such, the dissolution behavior should be very similar which would then lead to very similar crack tip chemistries. Making these analogies thus suggest that the crack tip reactions would be similar, indicating that the plateau is related to the diffusion of hydrogen through the fracture process zone.

UD-165 with a quenched and tempered martensitic microstructure and significantly lower $D_{eff,H}$ supports the notion that the observed plateau in FCGR is a combination of crack tip reactions that produce hydrogen and the diffusion of hydrogen through the fracture process zone. The rate limiting step must, therefore, be one of these two processes depending on microstructure, diffusivity of hydrogen and the environmental conditions.

The results of this analysis suggest that FCGR in ultra-high strength UD-165 appears to be controlled by the hydrogen diffusion process through the FPZ over a range of test conditions.

5. CONCLUSION

This report describes the work conducted to understand the performance of ultra-high strength UD-165 for drillstring applications in sour environments, with frequency a key mechanical testing variable and pH and temperature key environmental variables. The key findings of this work for UD-165 are summarized as shown below:

- FCGR of UD-165 in sour environments increased with decreasing frequency for a range of conditions at pH = 7. The FCGR vs. frequency plot exhibited a dependency of $f^{-0.5}$
- In higher pH environments, i.e., pH = 9 and 12, the FCGR did not strongly depend on frequency. This was either due to the mild environmental conditions or from crack closure phenomenon
- At 200°C, the FCGR vs. frequency at pH = 7 had a dependency of slope equal to f^{-1}; this suggested a change in failure mechanism from hydrogen diffusion assisted fatigue crack growth to a stress corrosion cracking mechanism

The results of the experimental program were fitted using three analytical models. The analysis results suggest that the rate limiting step in fatigue crack propagation of ultra-high strength UD-165 for the environmental test conditions used in this study is via the diffusion of hydrogen through the fracture process zone.

This page intentionally left blank

6. REFERENCES

ASTM Standard E18, 2008. Standard Test Methods for Rockwell Hardness of Metallic Materials; ASTM International: West Conshohocken, PA, 2008. DOI: 10.1520/E0018-08B. http://www.astm.org

ASTM Standard E399, Standard Test Method for Linear-Elastic Plane-Strain Fracture Toughness K_{Ic} of Metallic Materials; ASTM International: West Conshohocken, PA, 2009. DOI: 10.1520/E0399-12E2. http://www.astm.org

ASTM Standard E1019, 2008, Standard Test Methods for Determination of Carbon, Sulfur, Nitrogen, and Oxygen in Steel, Iron, Nickel, and Cobalt Alloys by Various Combustion and Fusion Techniques. ASTM International: West Conshohocken, PA, 2008. DOI: 10.1520/E1019-08. http://www.astm.org

Bristoll, P.; Roeleveld, J. Fatigue of offshore structures: effect of seawater on crack propagation in structural steel. Proceedings of Conf. European Offshore Steels Research; ECSC, 1978.

Buitrago, J.; Weir, M. S.; Kan, W. C. Effect of loading frequency on fatigue performance of risers in sour environment. Offshore Mechanics and Arctic Engineering Conference (OMAE 2004), Vol.III Materials Engineering, June 20–25, 2004; ASME: Vancouver, British Columbia, 2004; Paper 51641.

Eadie, R. C.; Szklarz, K. E. Fatigue crack propagation and fracture in sour dilute brine. Proceedings of Corrosion 99, NACE International, Houston, TX, 1999a; Paper No. 611.

Eadie, R. C.; Szklarz, K. E. Fatigue initiation and crack closure of low alloy steels in sour brine environments. Proceedings of Corrosion 99, NACE International, Houston, TX, 1999b; Paper No. 610.

Eadie, R. L.; Szklarz, K. E.; Sutherby, R. L. Corrosion fatigue and near-neutral pH stress corrosion cracking of pipeline steel in very dilute carbonate/bicarbonate with and without the presence of hydrogen sulfide using the compliance technique. Proceedings of Corrosion 2003, NACE International, Houston, TX, 2003; Paper No. 03527.

Gangloff. R. P. Corrosion Fatigue Crack Propagation in Metals. In *Environmentally Induced Cracking of Metals*; Gangloff, R. P., Ives, M. B., Eds.; NACE: Houston, TX, 1990; 55–109.

Gangloff, R. P. Science-Based Prognosis to Manage Structural Alloy Performance in Hydrogen. In *Hydrogen Effects on Materials;* Somerday, B. P., Sofronis, P.; Jones, R. H., Eds.; ASM International: Materials Park, OH, 2009; pp 1–21.

Gasem, Z. M. Frequency Dependent Environmental Fatigue Crack Propagation in 7xxx Alloy/Aqueous Chloride System. Ph. D. Thesis, University of Virginia, Charlottesville, VA, 1999.

Hammond, R. I.; Baxter, D. P. Corrosion Fatigue of Simulated C-Mn Steel HAZ's in Sour Produced Fluids. OMAE 2008 27th International Conference on Offshore Mechanics and Arctic Engineering (OMAE 2008), Estoril, Portugal, June 15–20, 2008; Paper OMAE 2008–57149.

Holtam, C. M.; Baxter, D. P.; Ashcroft, I. A.; Thompson, R. C. Effect of Crack Depth on Fatigue Crack Growth Rates for C-Mn Pipeline Steel in a Sour Environment. *International Journal of Fatigue* **2009,** 1–4.

Hudak, Jr., S. J.; Feiger, J. H.; Patton, J. A. The Effect of Cyclic Loading Frequency on Corrosion-Fatigue Crack Growth in High-Strength Riser Materials. 29th International Conference on Offshore Mechanics and Arctic Engineering (OMAE 2010), Shanghai, China, June 6–11, 2010; Paper OMAE2010-20705.

Krishnamurthy, R. Microstructure and Yield Strength Effects on Hydrogen Environment Fatigue of Steels. Ph. D. Thesis, University of Virginia, Charlottesville, VA, 1991.

Maddox, S. J.; Pargeter, R. J.; Woollin, P. Corrosion fatigue of welded C-Mn steel risers for deepwater applications: a state of the art review. 24th International Conference on Mechanics and Arctic Engineering (OMAE 2005), Halkidiki, Greece, June 12–16, 2005; Paper OMAE2005-67499.

Macdonald, K. A.; Bjune, J. V. Failure Analysis of Drillstrings. *Engineering Failure Analysis* **2007,** *14*, 1641–1666.

Thodla, R.; Gui, F.; Gordon, R.; Xia, J. Corrosion Fatigue Performance of Girth Welded X65 Seamless Pipe for Flowline. NACE International 2010, San Antonio, March 14–18, 2010; Paper #10311.

Turnbull, A. Comparison of Hydrogen Charging of Structural Steel by Crack Tip Processes and by Bulk Reactions in the Cathodic Protection of Corrosion Fatigue Cracks. *Scripta Metallurgica* **1986,** *20*, 365–369.

Turnbull, A.; Dolphin; S.; Rackley, F. A. Experimental Determination of the Electrochemistry in Corrosion Fatigue Cracks in Structural Steel in Artificial Seawater. *Corrosion* **1988,** *44*, 55–61.

Turnbull, A.; Saenz de Sanata Maria, M. Predicting the Kinetics of Hydrogen Generation at the Tips of Corrosion Fatigue Cracks. *Metallurgical Transactions A* **1988,** *19A*, 1795–1806.

Vaisberg, O.; Vincké, O.; Perrin, G.; Sarda, J. P.; Faÿ, J. B. Faitgue of Drilling: State of the Art. *Oil & Gas Science and Technology – Rev. IFP* **2002,** *57*, 7–37.

Webster, S. E.; Austen, I. M.; Rudd, W. J. *Fatigue, corrosion fatigue and stress corrosion of steels for offshore structures.* ECSC Steel Publications, European Commission: Brussels, 1985; ECSC Report No. EUR 9460.

Wei, R. P.; Gangloff, R. P. Environmentally Assisted Crack Growth in Structural Alloys: Perspectives and New Directions. In *Fracture Mechanics: Perspectives and Directions (Twentieth Symposium)*, ASTM STP 1020; Wei, R. P., Gangloff, R. P. Eds.; American Society for Testing and Materials: Philadelphia, 1989; pp 233–264.

Wei, R. P.; Shim, G. Fracture Mechanics and Corrosion Fatigue. In *Corrosion Fatigue: Mechanics, Metallurgy, Electrochemistry, and Engineering*, ASTMSTP 801; Crooker, T. W., Leis, B. N., Eds.; American Society for Testing and Materials, 1983; pp 5–25.

The National Energy Technology Laboratory (NETL) conducts cutting-edge energy research and technology development and analyzes energy systems and international energy issues for the U.S. Department of Energy. The NETL-Regional University Alliance (NETL-RUA) is an applied research collaboration that combines NETL's energy research expertise with the broad capabilities of five nationally recognized, regional universities: Carnegie Mellon University (CMU), The Pennsylvania State University (PSU), the University of Pittsburgh (Pitt), Virginia Polytechnic Institute and State University (VT), and West Virginia University (WVU), and the engineering and construction expertise of an industry partner (URS). The NETL-RUA leverages its expertise with current fossil energy sources to discover and develop sustainable energy systems of the future, introduce new technology, and boost economic development and national security.

Brad Tomer
Acting Director
Strategic Center for Natural Gas and Oil
National Energy Technology Laboratory
U.S. Department of Energy

Maria Vargas
Deputy Director
Strategic Center for Natural Gas and Oil
National Energy Technology Laboratory
U.S. Department of Energy

Roy Long
Technology Manager
Strategic Center for Natural Gas and Oil
National Energy Technology Laboratory
U.S. Department of Energy

Elena Melchert
Program Manager
Oil and Gas Production
Office of Fossil Energy
U.S. Department of Energy

Cynthia Powell
Director
Office of Research and Development
National Energy Technology Laboratory
U.S. Department of Energy

Timothy McNulty
Associate Vice-President for
Government Relations
Carnegie Mellon University

Henry Foley
Vice President for Research
The Pennsylvania State University

George Klinzing
Vice Provost for Research
University of Pittsburgh

Robert Walters
Vice President for Research
Virginia Tech

Fred King
Vice President for Research and
Economic Development
West Virginia University

Kevin Donovan
RES Program Manager
URS Corporation